CIMAC CONGRESS 25
ZURICH, MAY 19 – 23, 2025

2025 | 079

Numerical study on hydrogen-diesel and ammonia-diesel combustion in internal combustion engines

Simulation Technologies, Digital Twins and Complex System Simulation

Kenji Hiraoka, YANMAR HOLDINGS CO., LTD.

Takafumi Kamino, YANMAR HOLDINGS CO., LTD.
Daichi Matsunaga, YANMAR HOLDINGS CO., LTD.
Gin Morita, YANMAR HOLDINGS CO., LTD.
Takafumi Tentora, YANMAR HOLDINGS CO., LTD.
Kazuteru Toshinaga, YANMAR HOLDINGS CO., LTD.

This paper has been presented and published at the 31st CIMAC World Congress 2025 in Zürich, Switzerland. The CIMAC Congress is held every three years, each time in a different member country. The Congress program centres around the presentation of Technical Papers on engine research and development, application engineering on the original equipment side and engine operation and maintenance on the end-user side. The themes of the 2025 event included Digitalization & Connectivity for different applications, System Integration & Hybridization, Electrification & Fuel Cells Development, Emission Reduction Technologies, Conventional and New Fuels, Dual Fuel Engines, Lubricants, Product Development of Gas and Diesel Engines, Components & Tribology, Turbochargers, Controls & Automation, Engine Thermondynamis, Simulation Technologies as well as Basic Research & Advanced Engineering. For further information please visit https://www.cimac.com.

ABSTRACT

Hydrogen and ammonia are well known as promising energy sources to replace fossil fuels. However, hydrogen is characterized by its fast combustion speed, and this characteristic leads to the occurrence of the abnormal combustion or increase in NOx emission. Ammonia also has disadvantage such as low ignitability, low burning speed and high NOx emissions. Co-combustion with diesel fuel can compensate their disadvantages and enable to apply hydrogen and ammonia as a main fuel for internal combustion engines. Therefore, it is important to understand the combustion process in internal combustion engines. In this study, a dual-fuel combustion model and a new reaction mechanism were developed and implemented into 3D-CFD software. Hydrogen-diesel and ammonia-diesel combustion in internal combustion engines with intake port gas fuel injection were investigated by engine tests and numerical approaches.

For a hydrogen-diesel dual-fuel engine, a dual-fuel combustion model simulates the ignition of diesel pilot fuel by detailed chemical mechanics and the flame propagation of hydrogen combustion by G-equation model. Hydrogen/diesel dual-fuel simulations were performed for various hydrogen ratios based on experimental data. The simulations clarified the hydrogen-diesel dual-fuel combustion process in internal combustion engines. Dual-fuel combustion process was also investigated by observing OH* chemiluminescence in a rapid compression and expansion machine test.

Ammonia-diesel dual-fuel engine was also numerically investigated. Ammonia/n-heptane co-combustion emission phi-T map was generated by zero-dimensional chemical reaction simulation. The 3D-CFD simulation reproduced the cylinder pressure history and heat release rate for each experimental condition with high accuracy. These simulation results clarify that unburned ammonia remains in the narrow space where diesel spray is not distributed such as crevice volume, and nitrous oxide remains on the surface of unburned ammonia zone.

Through these simulations, hydrogen-diesel and ammonia-diesel combustion processes in internal combustion engines have been investigated and these future challenges have been clarified.

1 INTRODUCTION

Yanmar has announced that we will develop and market green powertrains that are compatible with various green energy sources, such as alternative fuels, engines, and fuel cell systems, without compromising customer convenience to achieve carbon neutrality by 2050. As part of YANMAR GREEN CHALLENGE 2050 [1], we are developing internal combustion engines compatible with carbon-free fuels such as hydrogen (H_2), ammonia (NH_3) and methanol (CH_3OH). These fuels have different combustion characteristics compared to conventional fossil fuels.

H_2 has a higher burning speed than conventional fossil fuels, and preventing abnormal combustion and reducing NOx emissions are issues to be addressed. Dual-fuel combustion with diesel fuel makes it easy to control the ignition and combustion of H_2. Figure 1 shows a diagram of a dual-fuel engine. H_2 is introduced into the cylinder with air, and diesel fuel is injected into the cylinder and ignited near top dead center (TDC). H_2 is also ignited with diesel fuel, and this system enables stable and controlled ignition. NH_3 has been investigated for use as an energy source in shipping because NH_3 is easier to store and has higher energy density than hydrogen. However, in addition to its high toxicity, NH_3 has a low burning speed and low ignitability, and nitrous oxide (N_2O) and nitrogen monoxide (NO) and nitrogen dioxide (NO_2) are generated as the result of NH_3 combustion. It is well known that N_2O has a high global warming coefficient. Although it is difficult to use pure ammonia in internal combustion engines due to its low reactivity [2-4], dual-fuel combustion with diesel fuel has the potential for practical use because a diesel micro pilot ignition system is well adapted for ocean-going vessels due to fuel redundancy and stable ignition for safe ship operation, as well as H_2.

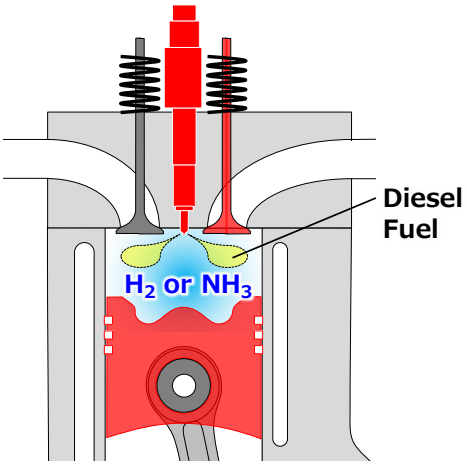

Figure 1. Schematic diagram of the dual-fuel engine configuration

Although many studies have demonstrated the potential of H_2/diesel and NH_3/diesel dual-fuel combustion engines [5-8], the dual-fuel combustion process in internal combustion engines is not yet fully understood. In this paper, we introduce our research activities for both H2/diesel and NH_3/diesel dual-fuel combustion [9-12]. The discussion of CH_3OH will be presented in another paper [13]. Dual-fuel combustion engine tests and numerical simulations for H_2/diesel and NH_3/diesel were conducted to investigate their combustion processes. Additionally, optical measurements and combustion model development for H_2/diesel dual-fuel combustion, as well as new reaction mechanism development for NH_3/diesel dual-fuel combustion, were carried out in order to improve the accuracy of our numerical simulations.

2 HYDROGEN AND DIESEL DUAL FUEL

2.1 Combustion analysis on OH* chemiluminescence images

To understand the H_2 and diesel dual-fuel combustion process experimentally, an optically accessible rapid compression and expansion machine (RCEM) that can simulate a single compression and expansion stroke was employed. Figure 2 shows a schematic of the experimental setup and illustrates the visualization area in the cylinder. The combustion chamber of the RCEM was modified from a naturally aspirated four-stroke-cycle single-cylinder diesel engine (Yanmar NFD170). A quartz window is installed on the cylinder head to visualize the combustion behavior via OH* (hydroxyl radical) chemiluminescence imaging. The technical specifications of the RCEM are shown in Table 1. During the combustion cycle, an air and H_2 mixture is introduced into the cylinder through the intake valve, and pilot diesel fuel is injected directly into the cylinder.

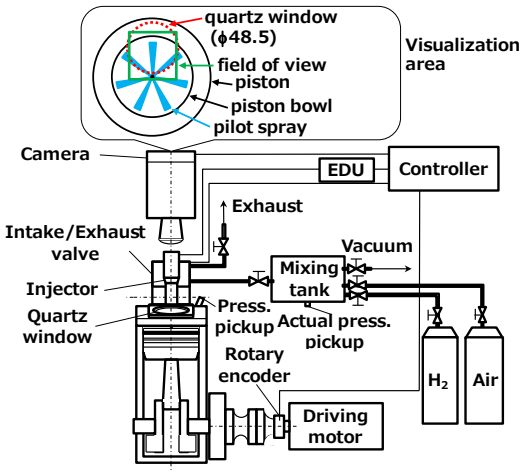

Figure 2. Schematic of the experimental setup of the RCEM and the visualization area in the combustion chamber

Table 1. Technical specifications of the RCEM

Bore x Stroke	102 x 105 mm
Compression ratio	15.4
Displacement	857 cc
Diesel injection system	Common rail system
Diesel injector nozzle	0.123mm x 7 holes

OH* imaging was performed for excess air ratio (λ_{total}) of 3. Figure 3 presents the in-cylinder pressure and heat release rate (HRR). Figure 4 presents the visualized images using OH* photography with respect to λ_{total} of 3. The excess air ratio for the H_2 alone (λ_{H_2}) was 3.6. In this study, the start of diesel injection was adjusted so that the ignition occurs near TDC.

Figure 4 shows that a bright region rapidly appears near the edge and inside the piston bowl after ignition. The bright regions then spread throughout the entire piston bowl until approximately 6.5 deg.aTDC (after top dead center), followed by the expansion of the low-brightness area from these regions toward the squish area. During this time, the heat release rate shows a peak value. After 10.5 deg.aTDC, the bright regions do not spread anymore and the heat release rate begins to decrease. It is difficult to distinguish between diesel combustion and hydrogen combustion; however, this test result clarifies the combustion process of diesel and H_2 dual-fuel combustion.

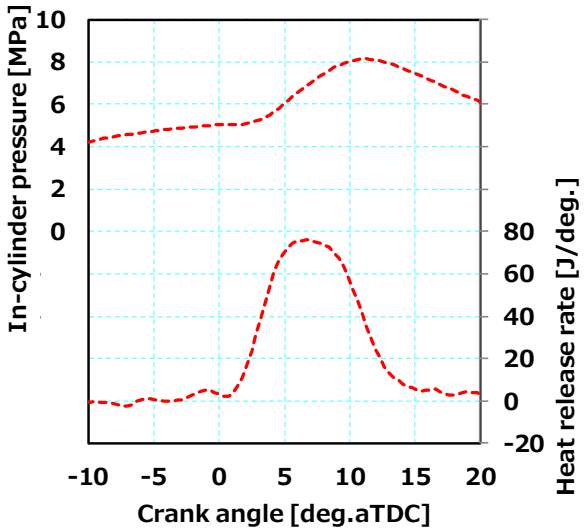

Figure 3. In-cylinder pressure and heat release rate for λ_{total} = 3

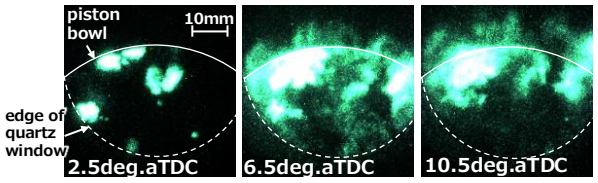

Figure 4. Visualized images using OH* photography with respect to λ_{total} = 3

2.2 Combustion modelling

To understand the H_2 and diesel dual fuel combustion process numerically, the dual-fuel combustion model suggested by Perini [10] was implemented into 3D-CFD software CONVERGE and applied to H_2 and diesel dual-fuel combustion. In this dual-fuel combustion model, the ignition of the pilot fuel is calculated using a detailed chemical reaction model by SpeedCHEM [14], and the flame propagation of the gas fuel is calculated using the G-equation model. Figure 5 shows a schematic diagram of the flame kernel determination in the dual-fuel combustion model. The cell types are divided into the DI zone, which contains a certain amount of direct injection fuel components, and the Premixed zone, which is composed almost entirely of gas fuel, and the Kernel cell, which is defined as the flame kernel.

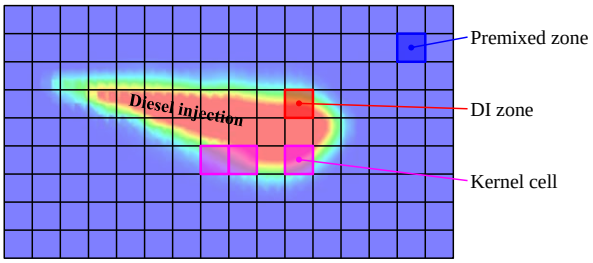

Figure 5. Schematic diagram of dual-fuel combustion model

The generation of the Kernel cell is determined by equation (1).

$$KI = \frac{S_{sp}}{S_L} \geq KI_{\text{flame}} \qquad (1)$$

In equation (1), S_L is the laminar burning speed, which is given by the following equation (2). For n_f fuels, including gas and liquid, the overall value is calculated from the laminar burning velocity $S_{Lf,i}$ of each fuel type i and the mass fraction $Y_{f,i}$.

$$S_L = \frac{\sum_{i=1}^{n_f} Y_{f,i}}{\sum_{i=1}^{n_f} \frac{Y_{f,i}}{S_{Lf,i}}} \qquad (2)$$

S_{sp} in equation (1) is shown by the following equation (3). Here, T is the temperature, and λ_e is derived by the eigenvalue calculation of equation (4) based on CEMA (Chemical Explosive Mode Analysis) [15]. In the eigenvalue calculation, $\boldsymbol{J}$ is the Jacobian matrix, $\boldsymbol{v}$ is the eigenvalue vector, and $\boldsymbol{\lambda}$ is a diagonal matrix with the eigenvalue λ_i as a component. $\boldsymbol{J}$ is shown by equation (5) using the mass fractions $Y_{s,i}$ and $Y_{s,j}$ of the chemical species i and j. λ_e is the maximum value of the real part of λ_i as shown in equation (6). If the number of cells V_k that satisfy equation (1) exceeds threshold ε_V, as shown in the following equation (7), the combustion model is changed to flame propagation mode.

$$S_{sp} = \left(\left| -\frac{1}{\lambda_e} \cdot \frac{400}{T(400+T)} \right| \|\nabla T\| \right)^{-1} \quad (3)$$

$$\boldsymbol{J} \cdot \boldsymbol{v} = \boldsymbol{\lambda} \cdot \boldsymbol{v} \quad (4)$$

$$\boldsymbol{J} = \frac{\partial}{\partial Y_{s,j}} \left(\frac{\partial Y_{s,i}}{\partial t} \right) \quad (5)$$

$$\lambda_e = \max\{\mathrm{Re}(\lambda_i), i = 1, \ldots\} \quad (6)$$

$$\frac{V_k}{V_{cyl}} \geq \varepsilon_V \quad (7)$$

2.3 Combustion analysis on 3D-CFD combustion simulations

Table 2 shows the experimental conditions for this study. To understand the hydrogen-diesel mixed combustion characteristics, the effect of the H_2 ratio ($GFER$: Gas Fuel Energy Ratio) was investigated through engine experiments. $GFER$ is defined by equation (8). Here, $\dot{m}$ is the mass flow rate, LHV is the lower heating value, and the subscripts indicate the fuel type.

Table 2. Experimental conditions of H_2/diesel dual-fuel engine

Engine speed	1200 min^{-1}
BMEP	1.0 MPa
Intake temperature	313 K
Intake pressure	240 kPa
Diesel Injection timing	-3 deg.aTDC
Diesel Injection pressure	80 MPa
Gas Fuel Energy Ratio	0 ~ 74%
Excess air ratio	2.7 ~ 2.3

$$GFER = \frac{\dot{m}_{H_2} \cdot LHV_{H_2}}{\dot{m}_{H_2} \cdot LHV_{H_2} + \dot{m}_{Diesel} \cdot LHV_{Diesel}} \quad (8)$$

Figure 6 provides an overview of the experimental equipment. H_2 and air are well mixed before the intake so that a homogeneous mixture in the cylinder is assumed in the engine test. The engine speed is kept constant at 1200 min^{-1}. The amount of fuel supplied was adjusted so that the BMEP remained constant at 1.0 MPa. The intake temperature, pressure, and diesel injection timing were kept constant, and the $GFER$ was varied in the range of 0 to 74% by adjusting the amount of H_2 and diesel fuel. As a result, the excess air ratio λ_{total} varied in the range of 2.7($GFER$ =0%) to 2.3($GFER$ =74%).

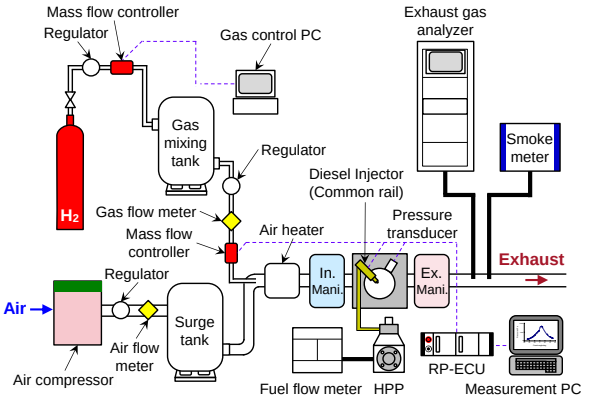

Figure 6. Overview of experimental equipment

Table 3 shows the simulation settings for this engine test. Converge v3.0.17, a 3D-CFD software from Convergent Science, was used. The dual-fuel combustion model described in the previous section was applied as the combustion model. The RNG k-ε model was used as the turbulence model, and the KH-RT (Kelvin-Helmholtz and Rayleigh-Taylor) model was used as the spray breakup model. In addition, the mechanism by Ren et al. [16], consisting of 178 chemical species and 758 reaction equations, was used as the chemical reaction model.

Table 3. Simulation conditions of H_2/diesel dual-fuel engine

Software	CONVERGE v3.0.17
Combustion model	Dual-fuel model (SpeedCHEM + G-Equation)
Turbulence model	RNG k-ε
Spray model	KH-RT
Chemical reaction model	multi-component mechanism by Ren

Figure 7 shows the validation results of in-cylinder pressure and heat release rate for each $GFER$ obtained in the H_2/diesel dual-fuel engine tests. After ignition, the heat release rate increases and reaches its first peak around 5 deg.aTDC under all conditions. The higher the $GFER$, the higher the observed peak value. After that, the heat release rate rises again and reaches a second peak around 10 deg.aTDC. At this time, the peak value is about the same regardless of $GFER$, but the peak timing is earlier under higher $GFER$ conditions. Then, the heat release rate decreases and follows a similar trend regardless of $GFER$, approaching 0 at around 40 deg.aTDC. As described above, it was found that the heat release rate changes depending on $GFER$ in H_2/diesel duel-fuel combustion. Next, the dual-fuel combustion process in the cylinder is investigated numerically.

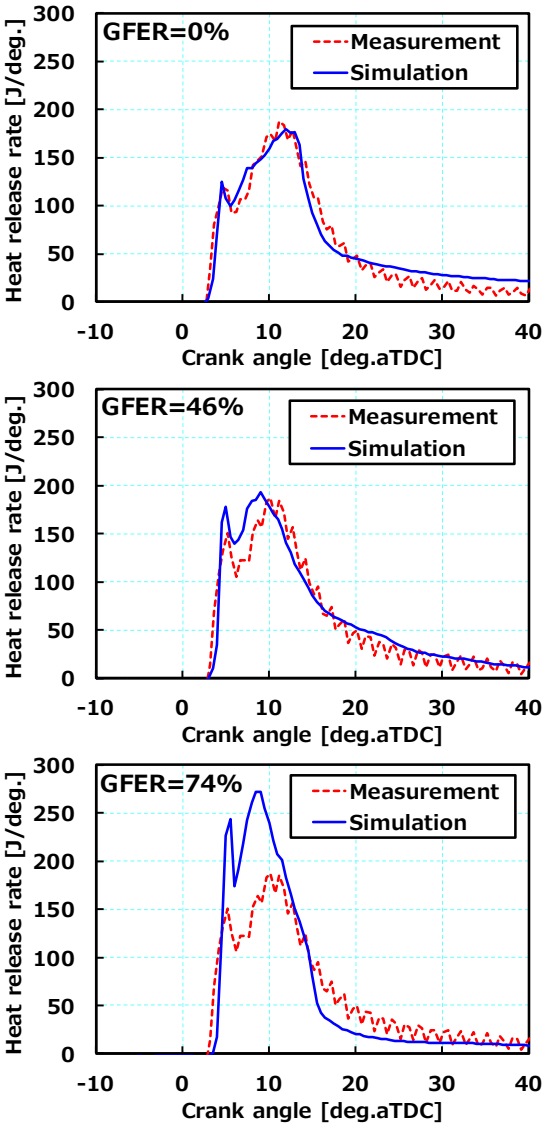

Figure 7. Comparisons of rate of heat release between experiment and simulation under $GFER$ = 0%, 46%, and 74% conditions

Figure 8 shows the isosurface of the equivalence ratio of 1 and the distribution of temperature under the conditions of $GFER$ 74%. At 4.0 deg.aTDC, which indicates the ignition timing, the heat release rate increases, and high temperature is observed inside the equivalence ratio of 1.0, which corresponds to the diesel spray. The heat release rate reaches its first peak at around 5.5 deg.aTDC. High temperature is observed throughout the diesel spray, and the surrounding hydrogen starts to be involved in the combustion. At 9 deg.aTDC, the diesel spray reaches the squish area, and the hydrogen flame is observed in the cavity area. After that, at 17 deg.aTDC, the hydrogen flame touches the cylinder liner, causing a decrease in the heat release rate. As seen in Figure 7, the flame propagation speed of hydrogen is overestimated under high $GFER$ conditions, and to solve this problem, it is necessary to improve the combustion model. In the future, we will investigate the dual-fuel combustion process further by combining optical measurements and 3D-CFD simulation results.

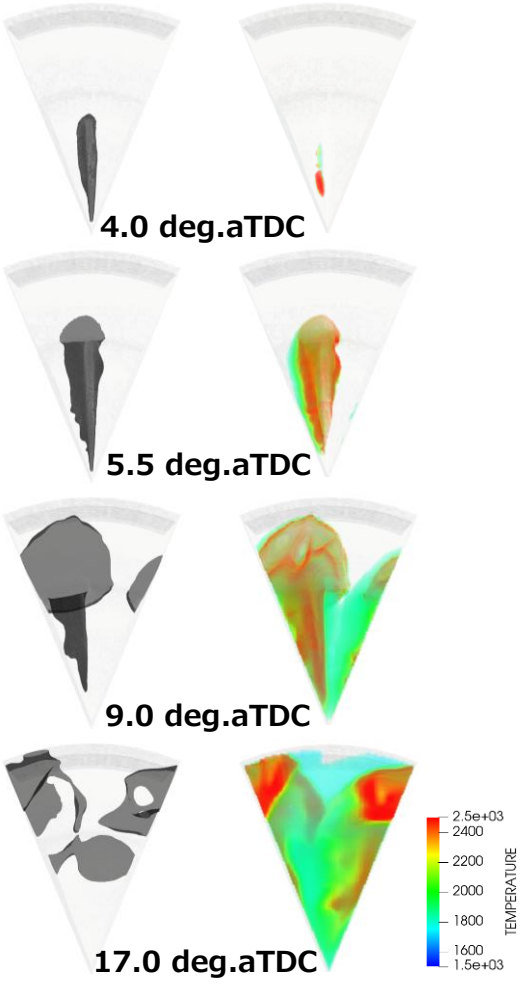

Figure 8. 3D visualization of H_2/diesel combustion process under $GFER$ = 74%: (left) isosurface for equivalence ratio of 1.0, (right) temperature

3 AMMONIA AND DIESEL DUAL FUEL

3.1 Reaction mechanism for *n*-heptane and ammonia combustion

A chemical reaction model for NH_3/*n*-heptane co-combustion was developed. The model is a combined model of the gasoline surrogate detailed kinetic model revision 2.0 (SIP-Gd2.0) [17] for the H_2-O_2 and hydrocarbon reaction subsets, the Nakamura model [18] for the NH_3 reaction subset, and the Glarborg model [19] for the reaction subsets for C1–C2 species and N-related species interactions. For the selection of individual reaction subsets, several reaction subsets were validated against weak flame locations in a micro flow reactor with a controlled temperature profile (MFR) [20]. The SIP-Gd2.0 model and the Nakamura model were chosen for use in the combined model because they showed the best reproducibility of the observed respective weak flame locations for *n*-heptane/air and NH_3/air mixtures in the MFR. The combined model comprises 887 species and 4277 reactions.

3.2 Emission characteristic for NH_3 co-combustion

A zero-dimensional chemical reaction simulation was carried out to clarify the characteristics of the combustion products from NH_3 under temperature and pressure conditions equivalent to those of a compression ignition engine. Reaction simulations were conducted under constant temperature and pressure conditions without accounting for temperature and pressure changes caused by chemical reactions. The pressure condition was set to 6.0 MPa, assuming the in-cylinder condition at the top dead center in a conventional compression ignition engine. The operation time was set to 1.0 millisecond, and the combustion products at the end of the calculation were arranged by equivalence ratio (φ) and temperature (T) conditions. The characteristics of the combustion products were investigated by generating a φ-T map, similar to the research previously conducted on diesel combustion [21] [22].

Figure 9 shows a φ-T map of the quantities of $NO+NO_2$, unburned NH_3, and N_2O in the ammonia-air mixture, and how the adiabatic flame temperature of the ammonia-air mixture varies with the equivalence ratio (for a pressure of 6 MPa and an initial temperature of 900 K). This φ-T map clarifies that $NO+NO_2$ is produced across a wide range of conditions from low to high temperatures, unlike conventional diesel combustion, which produces NOx at high temperatures above 2000 K. In ammonia combustion, NO is also produced in low-temperature conditions below 2000 K, with fuel NOx playing a large part in the production of $NO+NO_2$ at these lower temperatures. For equivalence ratios below 1.0, NH_3 remains unburned at low temperatures below 1500 K. At equivalence ratios above 1.0, it occurs at temperatures below 2200 K. N_2O, meanwhile, tends to increase at temperatures around 1500 K, regardless of the equivalence ratio. These results indicate that conventional lean combustion, running lean with an equivalence ratio of around 0.5, will not reduce $NO+NO_2$, and that low-temperature combustion will likely increase the amounts of unburned NH_3 and N_2O. The results also indicate the existence of a region where the quantities of $NO+NO_2$, unburned NH_3, and N_2O are all kept low by running rich with an equivalence ratio in the 1.2-to-1.5 range. These results agree with those obtained from a numerical simulation of a one-dimensional planar flame by Kobayashi et al. [23]. It can be concluded that a high equivalence ratio and high-temperature combustion can simultaneously inhibit emissions of $NO+NO_2$, unburned NH_3, and N_2O from ammonia combustion.

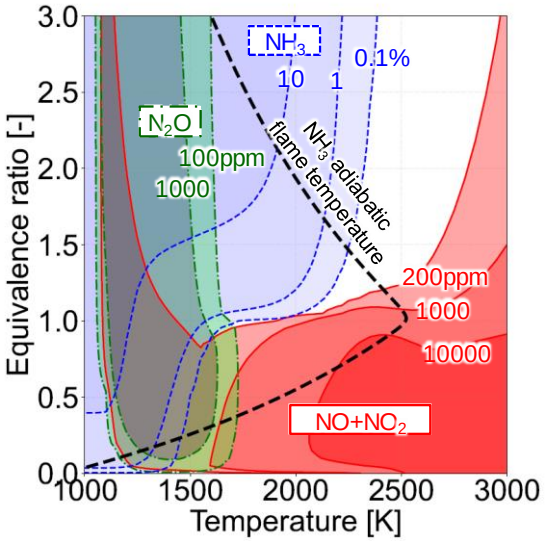

Figure 9. $NO+NO_2$, unburned NH_3, and N_2O emission characteristics of NH_3/air mixture with NH_3/air adiabatic temperature at each equivalence ratio, pressure of 6.0 MPa, and initial temperature of 900 K

3.3 Combustion analysis on 3D-CFD combustion simulations

The engine experiment and 3D-CFD simulation were performed to study combustion and emission characteristics for ammonia and diesel dual-fuel engines. Figure 10 shows a diagram of the experimental setup. Liquefied ammonia from a cylinder was vaporized and continuously supplied to the upstream end of the intake manifold while regulating the flow rate with a mass flow controller. The specifications of the engine experiments are shown in Table 4. The engine used in the

experiment was a single-cylinder diesel engine with a 94-mm bore and a 110-mm stroke. An NH_3/diesel dual-fuel engine experiment was conducted by injecting diesel fuel directly into the cylinder using a common rail direct injection system. An external air compressor was used on the air intake to achieve the required temperature and enable the pressure to be adjusted independently of the other engine operating conditions. A Fourier-transform infrared (FT-IR) spectrometer was used to analyze the composition of the exhaust gas.

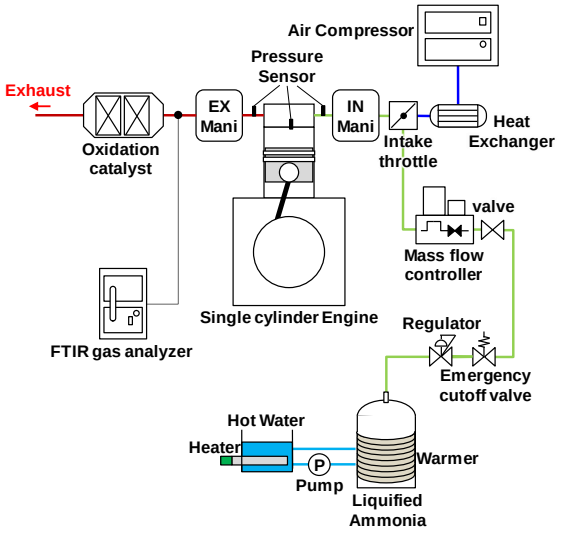

Figure 10. Outline of the experimental equipment for NH_3 and diesel dual-fuel engine

Table 4. Engine specification in NH_3 and diesel dual-fuel combustion

Number of cylinders	1
Bore [mm]	94
Stroke [mm]	110
Displacement [L]	0.76
Number of valves	4
Diesel fuel injection system	Common rail

This study involved varying the amounts of ammonia and diesel while operating the engine at a constant speed of 1200 min-1 with a constant load of 1.0 MPa, defined in terms of indicated mean effective pressure (IMEP). $GFER$ for NH_3 is the same as that for H_2. The injection pressure for diesel fuel is 80 MPa, and the injection timing for diesel fuel is adjusted to keep 50% burning point constant in any $GFER$. As aforementioned, in addition to the engine test, a detailed investigation of the combustion process and emission characteristics of the ammonia and diesel dual-fuel engine was carried out using the 3D-CFD simulation. The basic simulation setup is the same as for the H_2 and diesel dual-fuel case, as shown in Table 3. The differences are that SpeedCHEM [14] was used as the chemical reaction solver and the NH_3 and *n*-heptane chemical reaction model was applied in the NH_3 and diesel dual-fuel combustion case. In order to verify the accuracy of the 3D-CFD simulation, the simulation results were compared with engine experimental results. Figure 11 shows the comparison of in-cylinder pressure and heat release rate histories for $GFER$ = 0%, 55%, and 95%. The 3D-CFD simulation well reproduced the high heat release rate at the $GFER$ of 55% condition and the moderate heat release rate at $GFER$ = 95%, respectively. These simulation results show good agreement with the engine experimental results at any $GFER$ condition.

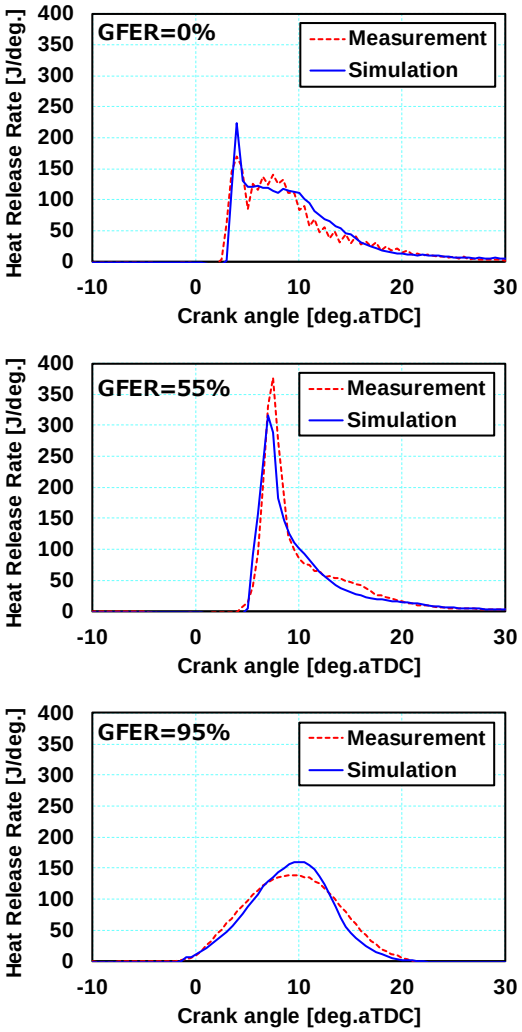

Figure 11. Validation of 3D-CFD simulation by the comparison of in-cylinder pressure and heat release rate history in the engine experimental results at $GFER$ = 0% and 55% and 95% respectively

The numerical simulation results were presented visually to enable a detailed study of the combustion process and the distribution of combustion products. Figure 12 shows the isosurface of an equivalence ratio of 1.0 and the three-dimensional temperature distribution in the combustion chamber for $GFER$ = 95%. An ammonia flame front can be seen close to the diesel fuel-air mixture when the crank angle is 5deg.aTDC, after which the ammonia flame spreads throughout the combustion chamber. Thus, the numerical simulation results provide a way to investigate how the ammonia flame spreads across the combustion chamber, with the injection of a very small amount of diesel serving as an ignition source.

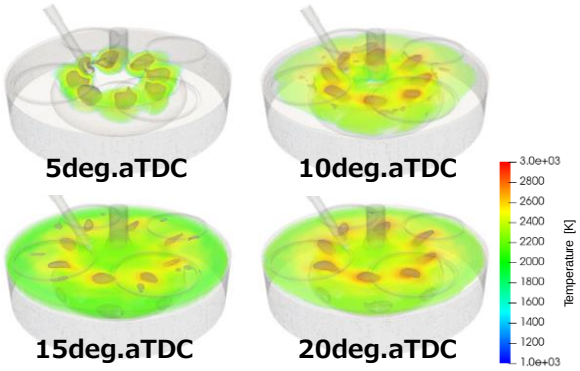

Figure 12. Isosurface of equivalence ratio 1.0 (gray) and temperature distribution at each crank angle at $GFER$ = 95%

N_2O and unburned NH_3 emissions were also compared with engine experimental results. Figures 13 and 14 show the comparison between 3D-CFD simulation results and engine experimental results for each $GFER$. The simulation results reproduce these emissions well both qualitatively and quantitatively for $GFER$ of up to 44%. N_2O emissions in the 3D-CFD simulation results show declines when $GFER$ exceeds 50% and do not coincide with engine experimental results. This indicates that further study of NH_3/*n*-heptane and air reactions in low-temperature conditions near the wall boundary is needed to understand the N_2O and unburned NH_3 emissions quantitatively.

Focusing on the in-cylinder distribution of unburned NH_3, NH_3 is consumed by combustion, but the ammonia flame does not propagate into narrow zones such as the crevice volume. A large amount of unburned NH_3 remains in such narrow zones at $GFER$ = 95%, as shown in Figure 15.

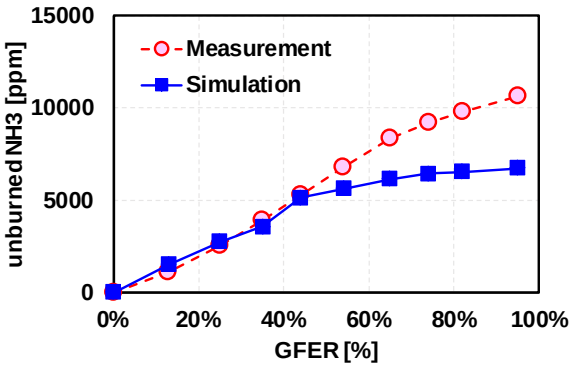

Figure 13. Comparison of unburned NH_3 emission between engine experiment and 3D-CFD simulation results at each $GFER$

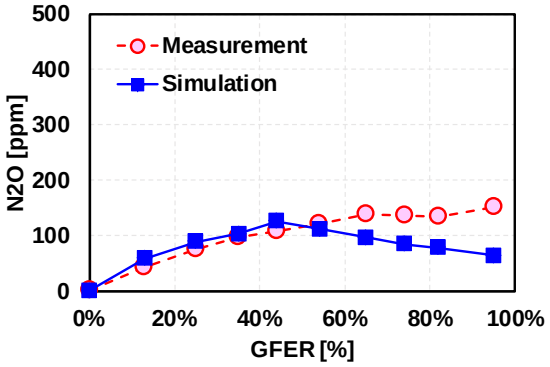

Figure 14. Comparison of N_2O emission between engine experiment and 3D-CFD simulation results at each $GFER$

Figure 15. Unburned NH_3 distribution estimated by 3D-CFD simulation at $GFER = 95\%$

Regarding N_2O, Figure 16 shows how N_2O is formed in the ammonia flame front. This N_2O is in turn decomposed inside the flame. The high temperatures inside the flame cause N_2O to decompose into N_2 and other species. In the vicinity of the combustion chamber walls, however, such as the crevice between the piston and liner,

residual N_2O is still present when combustion has completed at 20deg.aTDC due to the effects of the wall temperature. This is likely to be the reason why ammonia engines emit N_2O. In other words, this indicates that minimizing such crevices inside the combustion chamber should help to reduce N_2O emission.

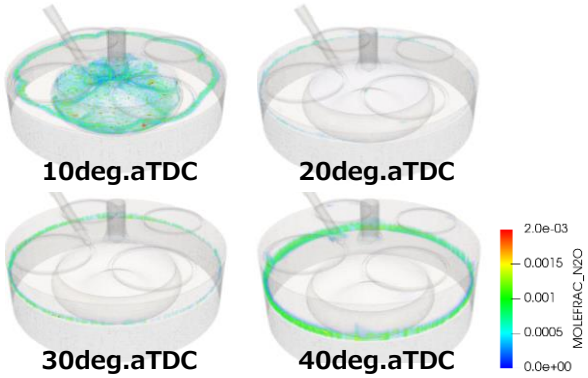

Figure 16. N_2O distribution estimated by 3D-CFD simulation the $GFER = 95\%$

4 CONCLUSIONS

This paper has described the development of optical measurement and numerical simulation for H_2/diesel and NH_3/diesel dual-fuel combustions as part of YANMAR's research activities toward carbon neutrality by 2050.

OH* imaging and numerical simulation have clarified the combustion process for H_2 and diesel dual-fuel engines. Both results show that the high-temperature region caused by the combustion first appears at the periphery of the piston bowl and spreads along its wall. H_2-diesel mixed combustion engine experiments were carried out in the range of $GFER$ = 0 to 74%. The heat release rate observed in the experimental results was well reproduced under each condition. Three-dimensional visualization of the simulation results showed that the initial heat release rate is higher under high $GFER$ conditions because diesel burns with surrounding H_2 after ignition, and that the second peak in the heat release rate occurs earlier due to interference between H_2 flame surfaces.

Regarding NH_3 combustion, an NH_3/*n*-heptane co-combustion chemical reaction model was developed by combining ammonia, *n*-heptane, and C-N reaction models. The φ-T map clarified emission characteristics for NH_3 combustion, and stoichiometric conditions are effective for reducing emissions of unburned NH_3 and N_2O. The 3D-CFD simulation well reproduced the engine experimental results and was able to clarify the combustion and emissions characteristics for ammonia and diesel dual-fuel combustion in internal combustion engines.

We believe that the numerical simulation technology introduced in this paper can be applied not only to hydrogen and ammonia but also to various alternative fuel engines such as methanol and other fuels. Toward a carbon-neutral society, we aim to develop competitive engines early and provide them to our customers and markets by utilizing these numerical simulation technologies.

5 ACKNOWLEDGMENTS

The authors would like to express sincere appreciation to Kyoto University for the H_2/diesel optical measurement, which was supported financially by The Nippon Foundation. Additionally, the authors would like to thank Wisconsin Engine Research Consultants for the development of the dual-fuel combustion model and Tohoku University for the development and validation of the NH_3/diesel chemical reaction mechanism.

6 REFERENCES

[1] YANMAR GREEN CHALLENGE 2050, https://www.yanmar.com/global/about/ygc/ (accessed on 04 December 2024)

[2] Cornelius, W., Huellmantel, L. and Mitchell, H. 1965, Ammonia as an engine fuel. SAE Technical Paper 650052.

[3] Pearsall, T. and Garabedian, C. 1967. Combustion of Anhydrous Ammonia in Diesel Engines, SAE Technical Paper 670947.

[4] Starkman, E., James, G. and Newhall, H. 1967. Ammonia as a Diesel Engine Fuel: Theory and Application, SAE Technical Paper 670946.

[5] Reiter, A. J. and Kong, S. 2011, Combustion and emissions characteristics of compression-ignition engine using dual ammonia-diesel fuel, Fuel, Volume 90, Issue 1, 2011, Pages 87-97.

[6] Niki, Y. 2023. Experimental and numerical analysis of unburned ammonia and nitrous oxide emission characteristics in ammonia/diesel dual-fuel engine. International Journal of Engine Research. 2023;24(9):4190-4203.

[7] Mante, T., Mestre, L., Seidel, L., Hoppe, A., Theile, M., Prehn, S., Mauss, F. and Buchholz, B. 2023. Numerical Study of NH3-Diesel Combustion in a Retrofit for Marine Engines using Detailed Kinetics, CIMAC Congress 2023 Proceedings No.426.

[8] Tsujimura, T. and Suzuki, Y. 2017. The utilization of hydrogen in hydrogen/diesel dual fuel engine, International Journal of Hydrogen Energy Volume 42, Issue 19, Pages 14019-14029.

[9] Mukhtar, G., Shimogawa, K., Horibe, N., Hayashi, J., Kawanabe, H., Morita, G. and Hiraoka, K. 2024. Combustion Analysis of Hydrogen-DDF Mode Based on OH* Chemiluminescence Images, SAE Technical Paper 2024-01-2367.

[10] Perini, F., Wright, C., Reitz, R., Hiraoka, K. and Kamino, T. 2024. A Dual-Fuel Model of Flame Initiation and Propagation for Modelling Heavy-Duty Engines with the G-Equation, SAE Int. J. Adv. & Curr. Prac. in Mobility 6(3):1380-1392.

[11] Murakami, Y., Nakamura, H., Tezuka, T., Hiraoka, K. and Maruta, K. 2022. Effects of mixture composition on oxidation and reactivity of DME/NH_3/air mixtures examined by a micro flow reactor with a controlled temperature profile, Combustion and Flame, 238, 111911.

[12] Hiraoka, K., Matsunaga, D., Kamino, T., Honda, Y., Toshinaga, K., Murakami, Y. and Nakamura, H. 2024. Experimental and numerical analysis on combustion characteristics of ammonia and diesel dual fuel engine, SAE Int. J. Adv. & Curr. Prac. in Mobility 6(3):1441-1458.

[13] Morimitsu, D., Toshinaga, K., Hiraoka, K., Matsunaga, D., Mimoto, R., Sato, Y. and Hamaoka, S. 2025. Development of 4-stroke medium speed methanol/diesel-fueled engine for marine application in YANMAR, CIMAC Congress 2025 Proceedings No.381.

[14] Perini, F., Galligani, E. and Reitz, R. 2012. An analytical Jacobian approach to sparse reaction kinetics for computationally efficient combustion modelling with large reaction mechanisms, Energy Fuels 2012, 26, 8, 4804–4822.

[15] Lu T.F., Yoo, C.S., Chen, J. H. and Law, C. K. 2010. Three-dimensional direct numerical simulation of a turbulent lifted hydrogen jet flame in heated coflow: a chemical explosive mode analysis. Journal of Fluid Mechanics. 2010;652:45-64.

[16] Ren, S., Kokjohn, S., Wang, Z., Liu, H., Wang B. and Wang, J. 2017. A multi-component wide distillation fuel (covering gasoline, jet fuel and diesel fuel) mechanism for combustion and PAH prediction, Fuel, Volume 208, 2017, Pages 447-468.

[17] Miyoshi, A and Sakai, Y. 2017. Construction of a Detailed Kinetic Model for Gasoline Surrogate Mixtures, Transactions of Society of Automotive Engineers of Japan, 48 (5), 1021-1026 [in Japanese].

[18] Nakamura, H., Hasegawa, S. and Tezuka, T. 2017. Kinetic modeling of ammonia/air weak flames in a micro flow reactor with a controlled temperature profile, Combustion and Flame. 2017;185:16-27.

[19] Glarborg, P., Miller, J. A., Ruscic, B. and Klippenstein, S. J. 2018, Modeling nitrogen chemistry in combustion, Progress in Energy and Combustion Science 67 (2018), 31-68.

[20] Maruta, K., Kataoka, T., Kim, N., Minaev, S. and Fursenko, R. 2005. Characteristics of combustion in a narrow channel with a temperature gradient, Proceedings of the Combustion Institute 30 (2005), 2429-2436.

[21] Akihama, K., Takatori, Y., Inagaki, K., Sasaki, S. and Dean, M. A., 2001. Mechanism of the Smokeless Rich Diesel Combustion by Reducing Temperature, SAE Technical Paper 2001-01-0655.

[22] Kamimoto, T. and Bae, M. 1988. High Combustion Temperature for the Reduction of Particulate in Diesel Engines, SAE Technical Paper 880423.

[23] Kobayashi, H., Hayakawa, A., Somarathne, K. D. K. A. and Okafor, E. C. 2019. Science and technology of ammonia combustion, Proceedings of the Combustion Institute, Volume 37, Issue 1, 2019, Pages 109-133.

7 CONTACT

Kenji Hiraoka
YANMAR HOLDINGS CO., LTD.
2481 Umegahara, Maibara, Shiga
521-8511, Japan
kenji_hiraoka@yanmar.com